

Resonant Bound-Free Contributions to Thomson Scattering of X-rays by Warm Dense Matter

W. R. Johnson

University of Notre Dame, Notre Dame, IN 46556

J. Nilsen, K. T. Cheng

Lawrence Livermore National Laboratory, Livermore, CA 94551

Abstract

Recent calculations [Nilsen et al. arXiv:1212.5972] predict that contributions to the scattered photon spectrum from $3s$ and $3p$ bound states in chromium ($Z = 24$) at metallic density and $T = 12$ eV resonate below the respective bound-state thresholds. These resonances are shown to be closely related to continuum lowering, where $3d$ bound states in the free atom dissolve into a resonant $l = 2$ partial wave in the continuum. The resulting d -state resonance dominates contributions to the bound-free dynamic structure function, leading to the predicted resonances in the scattered X-ray spectrum. Similar resonant features are shown to occur in all elements in the periodic table between Ca and Mn ($20 \leq Z \leq 25$).

Keywords: 52.25.Os: Emission, absorption and scattering of radiation, 52.38.-r: Laser-plasma interaction, 52.70.-m: Plasma diagnostic techniques, 56.65.Rr: Particle in cell method.

As discussed in the accompanying article Nilsen et al. [1], resonances in bound-free contributions to Thomson scattering of X-rays for a Cr plasma can complicate the determination of plasma density and temperature from measurements of the scattered X-ray spectrum. Inasmuch as bound-state features in dense plasmas of lighter elements show up as smooth broad features, it is of interest to explore the origin of the resonances that show up in Cr. To this end, we first note that the free Cr atom has the configuration $[Ar] 3d^5 4s$. In a dense plasma, the bound electrons outside the Ar-like ionic core dissolve into the continuum. In particular, the $3d$ electrons in Cr form a resonant state near 12 eV above threshold for the conditions considered here. It is the contribution of this d -state resonance that leads to resonances in the Thomson scattering

Email addresses: `johnson@nd.edu` (W. R. Johnson), `nilsen1@llnl.gov` (J. Nilsen), `ktcheng@llnl.gov` (K. T. Cheng)

Table 1: Properties of elements $20 \leq Z \leq 25$ at $T = 5$ eV. A is the atomic weight, ρ (g/cc) is plasma density, ϵ_{2s} and ϵ_{2p} are average-atom eigenvalues (eV) of $3p$ and $3s$ bound states, N_b and N_c are the number of bound and continuum electrons per ion. Z_i is the average ion charge. n_s , n_p and n_d are the number of continuum electrons in s , p and d states, respectively.

	Ca	Sc	Ti	V	Cr	Mn
Z	20	21	22	23	24	25
A	40.080	44.960	47.870	50.940	52.000	51.940
ρ	1.56	2.99	4.54	6.11	7.19	7.47
$-\epsilon_{3s}$	35.16	38.94	43.68	49.50	56.22	63.66
$-\epsilon_{3p}$	16.99	18.69	21.26	24.84	29.26	34.37
N_b	17.67	17.91	17.96	17.97	17.98	17.99
N_c	2.33	3.09	4.04	5.03	6.02	7.01
Z_i	1.45	2.00	2.24	2.56	2.65	2.32
n_s	0.298	0.389	0.419	0.474	0.511	0.507
n_p	0.459	0.572	0.606	0.691	0.744	0.709
n_d	1.343	1.933	2.852	3.698	4.611	5.676

cross section. In the following paragraphs, we study these resonances in greater detail for Cr and other elements between Ca and Mn ($20 \leq Z \leq 25$).

In Table 1, we show results from average-atom calculations of plasmas of elements in row four of the periodic table. In each case, we assume that the plasma density is the metallic density and that the plasma temperature is $T = 5$ eV. In the first four rows of the table, we list the atomic symbol, atomic number Z , atomic weight A and density ρ (g/cc). In the next two lines, we show average-atom eigenvalues ϵ_{3s} and ϵ_{3p} of $3s$ and $3p$ states (eV). The theoretical inner shell ionization thresholds $-\epsilon_{nl}$ are 20-30% smaller than measured values [2]. Rows seven and eight list N_b and N_c , the average number of bound and continuum electrons inside the Wigner-Seitz (WS) sphere. The average-atom model predicts that there are approximately 18 bound electrons and $Z - 18$ continuum electrons for each element. The ninth row gives Z_i , the average ionic charge or, equivalently, the number of free electrons per ion. For elements listed in the table, Z_i , which is near 2, is significantly smaller than N_c owing to the fact that the continuum charge is concentrated inside the WS sphere. In the final three rows of the table, we list n_s , n_p and n_d , contributions to N_c from s , p and d partial waves, respectively. It should be noted that these three partial-wave contributions account almost completely for N_c . Moreover, for the elements in question, d -states provide the dominant contribution to the sum. In summary, the continuum is concentrated inside the WS sphere and is dominated by d -state partial waves.

In Fig. 1, we plot the d -state phase shift $\delta_d(\epsilon)$ and the continuum d -wave distribution inside the WS sphere $n_d(\epsilon)$ for elements in Table 1. The distribution

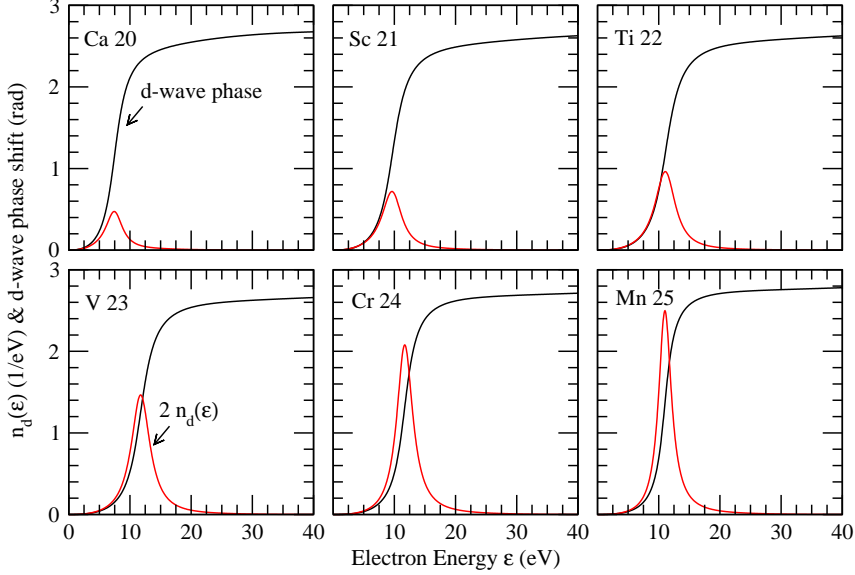


Figure 1: The d -state phase shift $\delta_d(\epsilon)$ and twice the continuum d -state distribution function $n_d(\epsilon)$ are shown as functions of electron energy ϵ (eV) for 5 eV plasmas at metallic density of elements in row four of the periodic table.

function $n_l(\epsilon)$ for a continuum state with angular momentum l is defined by

$$n_l(\epsilon) = \frac{2(2l+1)}{1 + \exp[(\epsilon - \mu)/kT]} \int_0^{R_{\text{ws}}} P_{pl}(r)^2 dr, \quad (1)$$

where $P_{pl}(r)$ is the radial wave function for a continuum state with momentum p and angular momentum l . When integrated over energy,

$$n_l = \int_0^\infty n_l(\epsilon) d\epsilon \quad (2)$$

gives the total number of continuum electrons for the s , p , d partial waves listed in the final three rows of Table 1. In all cases, the continuum d -waves exhibit resonant behavior near 12 eV, with strong peaks in the distribution functions $n_l(\epsilon)$ and corresponding changes in the phase shifts by almost a factor of π .

The contribution to the Thomson scattering dynamic structure function from bound states $S_b(k, \omega)$ is the sum over contributions from individual subshells with quantum numbers (n, l) :

$$S_b(k, \omega) = \sum_{nl} S_{nl}(k, \omega) \quad (3)$$

$$S_{nl}(k, \omega) = \frac{o_{nl}}{2l+1} \sum_m \int \frac{p d\Omega_p}{(2\pi)^3} \left| \int d^3 r \psi_p^\dagger(\mathbf{r}) e^{i\mathbf{k}\cdot\mathbf{r}} \psi_{nlm}(\mathbf{r}) \right|^2, \quad (4)$$

where $p = \sqrt{2(\omega + \epsilon_{nl})}$ is the momentum of the continuum electron, o_{nl} is the fractional occupation number of subshell (n, l) , and $\mathbf{k} = \mathbf{k}_0 - \mathbf{k}_1$ and $\omega = \omega_0 - \omega_1$ are the momentum and energy transfer from the incident photon (\mathbf{k}_0 , ω_0) to the scattered photon (\mathbf{k}_1 , ω_1), respectively. Atomic units in which $e = \hbar = m = 1$ are used here. In Eq. (4), $\psi_{\mathbf{p}}(\mathbf{r})$ is an average-atom wave function that approaches a plane wave $e^{i\mathbf{p}\cdot\mathbf{r}}$ asymptotically and $\psi_{nlm}(\mathbf{r})$ is the wave function for a bound state with quantum numbers (n, l, m) . The bound-state wave function is expressed in terms of the radial wave function $P_{nl}(r)$ as

$$\psi_{nlm}(\mathbf{r}) = \frac{1}{r} P_{nl}(r) Y_{lm}(\hat{r}). \quad (5)$$

Moreover, the scattering wave function, which consists of a plane wave plus an *incoming* spherical wave is expanded as

$$\psi_{\mathbf{p}}(\mathbf{r}) = \frac{4\pi}{p} \sum_{l_1 m_1} i^{l_1} e^{-i\delta_{l_1}} \frac{1}{r} P_{pl_1}(r) Y_{l_1 m_1}^*(\hat{p}) Y_{l_1 m_1}(\hat{r}), \quad (6)$$

where the radial function $P_{pl}(r)$ is normalized to a phase-shifted sine wave asymptotically:

$$P_{pl}(r) \rightarrow \sin(pr - l\pi/2 + \delta_l). \quad (7)$$

With the above definitions in mind, Eq. (4) can be expressed as

$$S_{nl}(k, \omega) = \frac{2p}{\pi} o_{nl} \sum_{l_1 l_2} A_{l_1 l_2} |I_{l_1 l_2}(p, k)|^2, \quad (8)$$

where

$$I_{l_1 l_2}(p, k) = \frac{1}{p} e^{i\delta_{l_1}(p)} \int_0^{R_{WS}} dr P_{pl_1}(r) P_{nl}(r) j_{l_2}(kr) \quad (9)$$

and

$$A_{l_1 l_2} = (2l_1 + 1)(2l_2 + 1) \begin{pmatrix} l_1 & l & l_2 \\ 0 & 0 & 0 \end{pmatrix}^2. \quad (10)$$

As shown earlier, the dominant contribution to the continuum wave function $P_{nl_1}(r)$ is from *d* waves ($l_1 = 2$) and occurs near continuum energy $\epsilon_p = p^2/2 \approx 12$ eV above threshold. It follows that the dominant contribution to $S_{3p}(k, \omega)$ is from the two terms with $(l_1, l, l_2) = (2, 1, 1)$ and $(2, 1, 3)$, while the dominant contribution to $S_{3s}(k, \omega)$ is from the single term $(l_1, l, l_2) = (2, 0, 2)$. Energy conservation implies that the resonant contribution to the scattered photon spectrum from bound state nl occurs at scattered X-ray energy $\omega_1 = \omega_0 + \epsilon_{nl} - \epsilon$, with $\epsilon \approx 12$ eV.

As a specific example, we consider scattering of a 4750 eV photon at 40° from Cr at metallic density and $T = 5$ eV. In the left panel of Fig. 2, we show the bound-free contribution $S_b(k, \omega)$ to the dynamic structure function. The vertical construction lines show the $2s$ and $2p$ resonance peaks and thresholds. The resonance peaks are shifted 12 eV below the thresholds of 29.3 and 56.2 eV

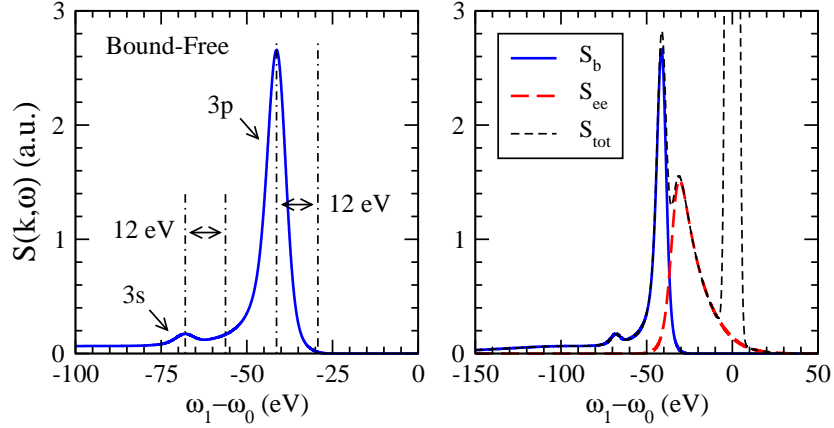


Figure 2: Left panel: $S_b(k, \omega)$ for Cr at metallic density and $T = 5$ eV is plotted against $\omega_1 - \omega_0$, where ω_1 is the scattered photon energy. The incident photon energy is $\omega_0 = 4750$ eV and the scattering angle is 40° . Resonance peaks and thresholds associated with transitions from $3s$ and $3p$ bound states are shown by the vertical construction lines. Right panel: Contributions from bound-free S_b , free-free S_{ee} , and the total structure function S_{tot} , which includes elastic scattering, are plotted against $\omega_1 - \omega_0$.

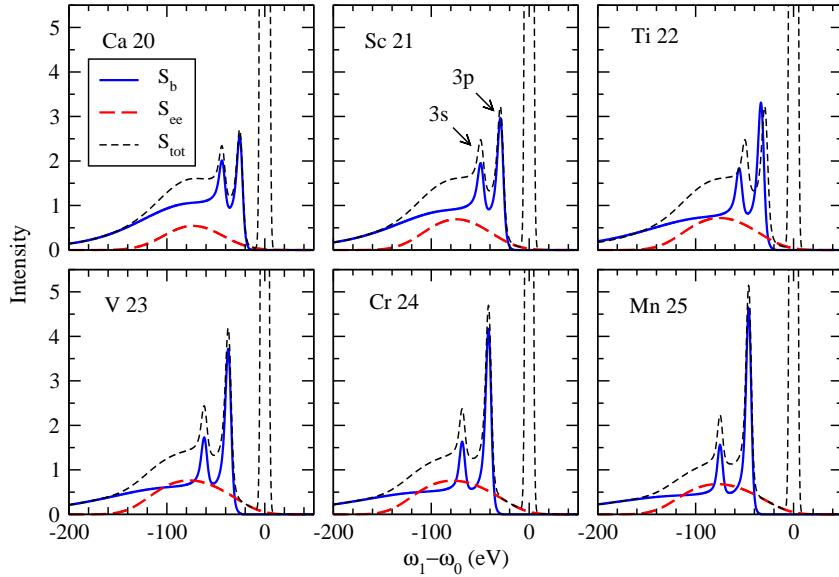


Figure 3: The dynamic structure function $S_{tot}(k, \omega)$ (short black dashes), bound-free contributions including $3s$ and $3p$ resonances $S_b(k, \omega)$ (solid blue lines) and free contributions $S_{ee}(k, \omega)$ (long red dashes) for scattering from elements listed in Table 1 are plotted as functions of $\omega_1 - \omega_0$, where ω_1 is the scattered X-ray energy and $\omega_0 = 4750$ eV is the incident X-ray energy. The scattering angle for the illustrated cases is 130° .

for the $3s$ and $3p$ electrons, respectively, as expected from the position of the peak in $n_d(\epsilon)$ shown in the Cr panel of Fig. 1.

In Fig. 3, we present results of calculations of the inelastic bound-free contribution to the dynamic structure function $S_b(k, \omega)$, the inelastic free-free contribution $S_{ee}(k, \omega)$ and the total dynamic structure function including elastic scattering $S_{tot}(k, \omega)$ for elements listed in Table 1. The incident X-ray energy in these examples is $\omega_0 = 4750$ eV and the scattering angle is 130° . The relative amplitude of the resonant peaks is seen to increase systematically throughout the sequence as expected from the d -electron distributions shown in Fig. 1. By contrast, the relative amplitude of the free-free contribution remains relatively constant from element to element as a consequence of the fact that Z_i , the number of free electrons per ion, is relatively constant throughout the sequence.

In conclusion, the resonances predicted in the bound-free contribution to the Thomson scattering X-ray spectrum arise from a d -state resonance in the continuum associated with continuum lowering in a dense plasma. For the examples considered herein, elements between Ca and Mn at metallic density and $T = 5$ eV, the d -state resonances occur at continuum-electron energy $\epsilon \approx 12$ eV. The amplitude of the d -state resonances increase systematically from element to element. The d -state resonance dominate the continuum and the bound-free contribution to the dynamic-structure function $S_b(k, \omega)$. The resonance associated with transitions from subshell nl occurs at scattered X-ray energy $\omega_1 = \omega_0 + \epsilon_{nl} - \epsilon$, where the resonance energy for the cases considered here is $\epsilon \approx 12$ eV.

Acknowledgements

The authors owe a debt of gratitude to T. Döppner for bringing up the question of the origin of the resonances predicted in average-atom calculations. The work of J.N. and K.T.C. was performed under the auspices of the U.S. Department of Energy by Lawrence Livermore National Laboratory under Contract DE-AC52-07NA27344.

References

- [1] J. Nilsen, W. Johnson, K. T. Cheng, The effect of bound states on X-ray Thomson scattering for partially ionized plasmas, HEDP submitted for publication, [arXiv:1212.5972](https://arxiv.org/abs/1212.5972).
- [2] physics.nist.gov/PhysRefData/FFast/html/form.html.